applied sciences

MDPI

Article

A Multi-Analytical Approach for the Characterization of Archaeological Plant-Based Fibers and Residues: The Case of Oluz Höyük (North–Central Anatolia)

İrem Ceran [1,2,*], Ersin Kaygisiz [1,3], Mona Saba [4] and Şevket Dönmez [4]

[1] Research Center for the Conservation of Cultural Property of Foundation, Fatih Sultan Mehmet Vakıf University, Istanbul 34015, Türkiye; ersinkygsz@gmail.com or ersin.kaygisiz@istanbul.edu.tr
[2] Department of Restoration and Conservation of Cultural Assets, Faculty of Arts, Design and Architecture, Fatih Sultan Mehmet Vakıf University, Istanbul 34015, Türkiye
[3] Division of Turkish and Islamic Archaeology, Department of Archaeology, Faculty of Letters, Istanbul University, Istanbul 34459, Türkiye
[4] Department of Protohistory and Near Eastern Archaeology, Faculty of Letters, Istanbul University, Istanbul 34453, Türkiye; monasaba@istanbul.edu.tr (M.S.); sedon@istanbul.edu.tr (Ş.D.)
* Correspondence: iceran@fsm.edu.tr

Abstract

This study presents a multi-analytical approach for the characterization of plant-based archaeological remains, including bast fibers and seed coats, recovered from hearth soils, ash deposits, and ceramic contexts at Oluz Höyük (north–central Anatolia). The proposed protocol integrates stereomicroscopy, SEM-BSE imaging, ATR-FTIR spectroscopy, and TG/DTG analysis to assess the preservation state, microstructural features, and compositional properties of lignocellulosic materials in archaeological environments. Microstructural observations revealed striations, lumen channels, and fiber bundles consistent with plant-derived lignocellulosic bast-like fibers. Although some morphological characteristics are comparable to those reported for cultivated fiber plants such as hemp and flax, the applied analytical methods do not permit definitive species-level identification. SEM-BSE imaging further identifies well-preserved seed coats with diagnostic surface ornamentation. FTIR spectra exhibit characteristic bands associated with cellulose and lignin, confirming the presence of lignocellulosic tissues. TG/DTG analysis of associated ceramic residues indicates firing temperatures in the range of ~690–720 °C and highlights compositional variability related to raw material selection and depositional conditions. The results demonstrate the applicability of the proposed multi-analytical framework for the characterization and assessment of plant-derived archaeological materials while highlighting the limitations of species-level identification based solely on morphological, spectroscopic, and thermal analyses. This approach provides a reproducible methodology for investigating organic remains in complex archaeological matrices and contributes to the broader understanding of ancient material technologies.

Keywords: Oluz Höyük; Iron Age; Achaemenid Period; archaeometry; ATR-FTIR; archaeobotany

Check for updates

Academic Editor: Gino Iannace

Received: 15 May 2026
Revised: 3 July 2026
Accepted: 20 July 2026
Published: 14 October 2026

Copyright: © 2026 by the authors. Licensee MDPI, Basel, Switzerland. This article is an open access article distributed under the terms and conditions of the Creative Commons Attribution (CC BY) license.

1. Introduction

The Black Sea coasts, east–central Anatolia, and Iran are geographically connected through the Amasya region, making this area an important archaeological crossroads. Oluz

Höyük, where systematic archaeological excavations have been conducted since 2007, is one of the most significant ancient settlements reflecting this rich cultural landscape.

Located in north–central Anatolia (Figure 1), Oluz Höyük lies within the territory of the Gökhöyük Agricultural Enterprise Directorate (TİGEM), approximately 27 km along the Amasya–Çorum highway. The mound is situated on the western edge of the fertile Geldingen Plain. It lies south of the Çekerek River (Zuliya in Hittite texts; ancient Skylax), one of the principal tributaries of the Yeşilırmak River (Kummesmaha in Hittite texts; ancient Iris). The site is positioned approximately 2 km northwest of Gözlek village, 5 km east of Oluz village, and 3 km south of the Amasya–Çorum highway.

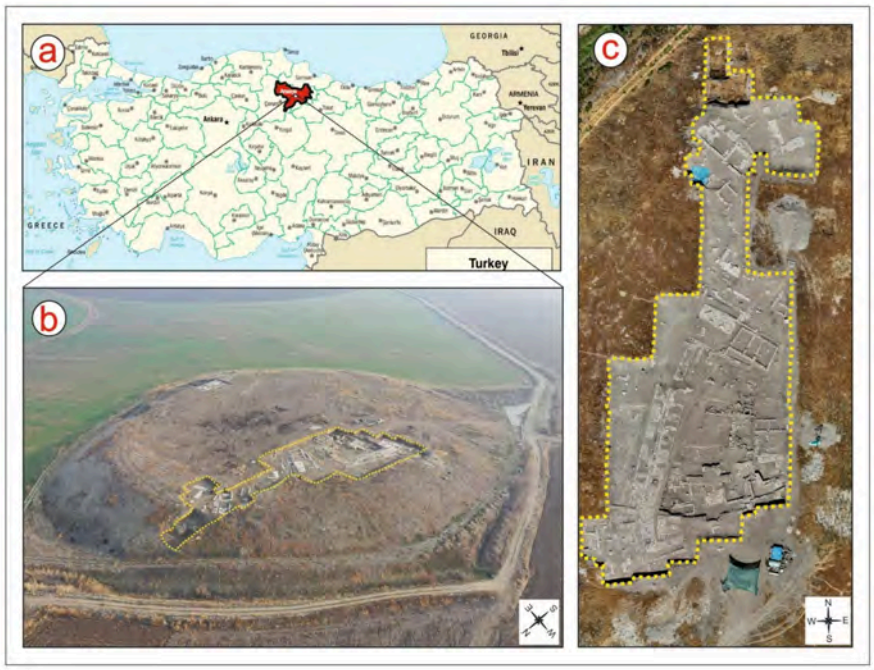


Figure 1. (**a**) Location map of Oluz Höyük in Amasya Province; the red-highlighted area indicates Amasya Province, and the star marks the location of Oluz Höyük; (**b**) aerial view of Oluz Höyük from the northwest, with the yellow dotted line outlining Trench A; (**c**) orthophoto of Trench A, whose boundaries are indicated by the yellow dotted line.

Oluz Höyük measures approximately 280 m in diameter and rises about 15 m above the surrounding plain (478.78 m above sea level), covering an area of nearly 45 decares. After eighteen excavation seasons [1–21], archaeological investigations have demonstrated that the settlement comprises ten superimposed occupational phases and maintained a continuous religious character throughout its long occupational history.

During the 2021 excavation season, stepped deepening works carried out at the northernmost edge of Trench A, the largest excavation area at Oluz Höyük, revealed intriguing remains belonging to the Collapse Period (ca. 1200–1150 BCE), which witnessed the fall of the Hittite Great Kingdom. Among the finds uncovered in the 7B2 Architectural Layer, particularly noteworthy are carbonized seed remains of wheat and vetch, associated with a religious ritual performed through burning. These findings appear to provide the first opportunity to recognize the rituals and practices of a new belief system that emerged during the process of the Hittite collapse. Approximately 600 years after the Hittite downfall, Oluz Höyük became an important religious center during the Phrygian Kingdom. The most significant structure pointing to this transformation is the Kubaba (Mother Goddess) Sanctuary, unearthed in the 4B Architectural Layer and dated to around 620 BCE. The sanctuary is observed to consist of a cella and altars (sacrificial platforms) of various sizes. Excavations at Oluz Höyük have begun to reveal previously unknown connections between

the Late Iron Age culture of north–central Anatolia and by extension, the Kızılırmak Basin and the East. In the 2B Architectural Layer (ca. 450–300 BCE), within the Achaemenid (Persian) strata, significant and unique archaeological finds have been identified that point to Archaic Monotheism. In this belief system, whose core practice was centered on the Fire Cult, structures such as an Atashkade (fire temple), a place of worship, areas for storing sacred ashes, and bothroi containing buried ritual objects, as well as finds associated with the cult of wine and water and with sacrificial pits, collectively demonstrate the existence of Archaic Monotheism. These discoveries indicate the institutionalization of a monotheistic faith at Oluz Höyük beginning in the 5th century BCE [6]. Another area of study involves textile remains recovered from archaeological layers. The preservation of such remains typically occurs under extreme environmental conditions. While dry frozen soils and water-logged contexts provide the most favorable environments for the survival of textiles, they may also be preserved in burnt layers through carbonization. Over the past two decades, textile studies conducted on materials unearthed during archaeological excavations have come to be regarded as a reliable source of archaeological knowledge. Since the fibers are usually found in a degraded and fragmentary state, their analyses greatly benefit from interdisciplinary approaches that combine analytical methods, experimental research, and the application of advanced technological knowledge. The rarity of textile remains or fibers in excavation contexts further enhances their value as a source of archaeological information.

The systematic archaeological excavations currently being developed at Oluz Höyük have already begun to make significant contributions to the archaeology of the Anatolian Iron Age, particularly in its religious dimension. Findings related to two missing links in the history of protohistoric Anatolian religion, namely the Cult of Kubaba (Architectural Layers 4A–B, ca. 620–500 BCE) and Early Zoroastrianism (Architectural Layer 2B, ca. 450–300 BCE), have been identified in the Iron Age architectural strata of Oluz Höyük. In addition, the Persian Period, characterized by the Basileion (local palace), the Persian Road, defensive structures, workshops, kitchens, and the Ahura Mazda Temple, is being investigated within the 2B Architectural Layer [1–21]. During excavations aimed at determining the eastern boundaries of the Ahura Mazda Temple, composed of an Atashkade (fire temple) and a place of worship, meticulous work in trench K18 uncovered the remains of a hearth. Advanced analyses conducted on the carbonized soil remains from this feature have provided valuable insights into new religious practices in Iron Age Anatolia. Furthermore, in the Northern Workshop structure emerging at the northern section of Trench A, a group of in situ pottery vessels was studied by collecting sample materials through light scraping of their inner surfaces. All of these analyses will be evaluated not only in relation to religious practices but also within the broader framework of production and subsistence economy in the Persian-period settlement.

Archaeological Context

In the systematic archaeological excavations at Oluz Höyük, initiated in 2007, a total of eleven main architectural layers have been identified. Layer 0 corresponds to the Medieval and Early Modern periods (13th–16th centuries CE), while the 1st Architectural Layer dates to the Hellenistic period (200–47 BCE). The 2A Architectural Layer belongs to the Late Phase of the Late Iron Age (300–200 BCE), and the 2B Architectural Layer to an earlier phase of the Late Iron Age (450–300 BCE). The 3rd Architectural Layer is likewise assigned to the Late Phase of the Late Iron Age (500–450 BCE). The 4A Architectural Layer belongs to the Early Phase of the Late Iron Age (550–500 BCE), while the 4B Architectural Layer is again attributed to the Early Phase of the Late Iron Age (ca. 620/600–550 BCE). The 5A Architectural Layer dates to the second half of the 7th century BCE (Middle Iron Age), and the 5B Architectural Layer to the first half of the 7th century BCE (Middle Iron Age). The 6A Architectural Layer is assigned to the 8th century BCE (Middle Iron Age), and the 6B

Architectural Layer to the 9th century BCE (Middle Iron Age). The 7A Architectural Layer, first identified in the 2014 field season, is dated to the 10th–11th centuries BCE (Early Iron Age/Dark Age), whereas the 7B Architectural Layer can be placed in the 12th century BCE (Dark Age). Layer 8 (13th century BCE) and Layer 9 (14th–15th centuries BCE) belong to the Late Bronze Age, that is, to the period of the Hittite Great Kingdom. Layer 10, based primarily on the evaluation of stone molds, flint tools, and pottery sherds, can be broadly dated to the Early Bronze Age II–III (mid-3rd millennium BCE). The analytical results presented in this article derive from the 2B Architectural Layer (Table 1) [1–21].

Table 1. Stratigraphy and Chronological Sequence of Oluz Höyük.

Period	Architectural Layer	Dates	Trench
Medieval Period	0	10–14th c. AD	A
Hellenistic Period	1	200–47 BC	A, B, C
Post-Achaemenid Period	2A	300–200 BC	A, B, C
Achaemenid Imperial Period	2B	450–300 BC	A, B, C
Achaemenid Imperial Period	3	500–450 BC	A, B, C, D
Late Iron Age	4A	550–500 BC	A, B
Medes Kingdom Period	4B	600–550 BC	A
Kashki Period 4	5A	650–600 BC	A, B
Kashki Period 3	5B	700–650 BC	A, B
Kashki Period 2	6A	8th c. BC	A, B
Kashki Period 1	6B	9th c. BC	A, B
Dark Age 2	7A	11–10th c. BC	A, B
Dark Age 1	7B1	1150–1100 BC	A, B
Late Hittite Transition Period	7B2	1200–1150 BC	A, B
Hittite Empire Period	8	13th c. BC	B
Hittite Empire Period	9	15–14th c. BC	B
Early Bronze Age II–III	10	Mid-3rd Millennium BC	B
Late Chalcolithic Period	11	Mid-4th Millennium BC	B

2. Materials and Methods

During the expansion and deepening works carried out in square K18, one phase of the 2B Architectural Layer excavations of the mound, a hearth area was uncovered. This hearth, coded as feature b.3828, was observed to be bounded on its northern side by a neatly cut stone block measuring 0.80 m in length and 0.20 m in thickness. Sieving and flotation analyses conducted on the soil samples taken from the hearth revealed a large number of carbonized seed grains as well as seed coat fragments [22]. This soil sample was included in the study with the consideration that other organic remains might also be present. The analytical dataset comprised archaeological materials representing different categories recovered from the 2B Architectural Layer of Oluz Höyük. The analyzed materials included hearth soil and ash deposits, three ceramic surface residue samples (collected from a bowl, a pot, and a jug), five isolated plant fiber specimens, one charred fiber fragment, one seed coat

fragment, and charred seed remains. This sampling strategy was designed to encompass a range of archaeological contexts and preservation states, thereby enabling a comparative multi-analytical assessment of plant-derived archaeological remains.

Likewise, during the excavations of the 2B Architectural Layer, deepening and expansion works at the northern end of Trench A and in square K10, located in the northwestern part of the mound, uncovered a workshop structure that included a kiln made of clay. On the floor of the workshop, an in situ assemblage consisting of a large clay bowl, a jar-shaped vessel, and a jug was revealed (Figure 2). Examination of the technical features of these vessels suggests that all were carefully produced for the storage and preservation of liquids. Soil samples taken from the interior surfaces of these ceramic vessels where they had been in direct contact with material, together with powder samples obtained by lightly scraping the ceramic surfaces with a scalpel at the same contact points, were collected for analysis and subjected to the necessary examinations [22].

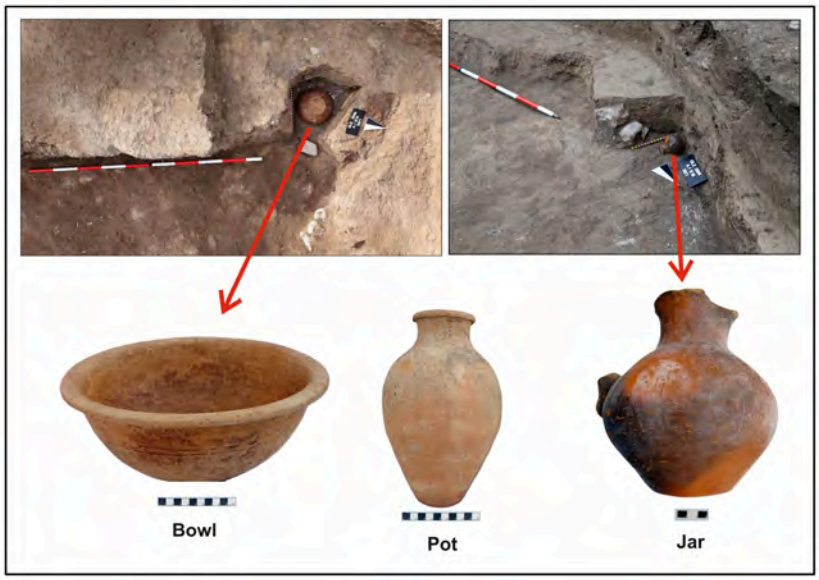


Figure 2. Ceramic samples excavated during the fieldwork and analyzed for smear samples [22].

2.1. Analytical Techniques

2.1.1. TG Analysis

Thermogravimetric analysis (TG) measurements were performed using a simultaneous thermal analyzer (Discovery SDT 650, TA Instruments, New Castle, DE, USA) to examine the thermal behavior and estimate the firing temperatures of the ceramic samples. Approximately ~10 mg of powdered sample was placed in an alumina crucible and heated from room temperature to 1000 °C at a constant heating rate of 10 °C/min under ambient-air atmosphere with a flow rate of 100 mL/min. The weight loss (TG) and derivative weight loss (DTG) curves were recorded and interpreted to identify decomposition stages and phase transformations. The interpretation focused on the relative positions of major thermal events and decomposition stages observed among the analyzed archaeological samples. Considering the limited number of independent specimens and their heterogeneous archaeological preservation, the TG/DTG results were interpreted comparatively rather than statistically. Samples were selected based on their archaeological context, state of preservation, and visible presence of organic remains. Particular attention was given to specimens exhibiting preserved fibrous morphology, carbonized plant tissues, or visible residues adhering to ceramic surfaces, as these materials were considered most suitable for archaeometric characterization. Thermal analyses were performed under identical

experimental conditions for all analyzed samples to ensure methodological consistency and comparability of the TG/DTG profiles.

2.1.2. ATR-FTIR Analysis

The characterization of the archaeological samples was conducted using Attenuated Total Reflectance Fourier Transform Infrared Spectroscopy (ATR-FTIR), focusing on the identification of both organic and inorganic constituents. Prior to analysis, all soil and smear samples were finely ground to ensure optimal contact with the ATR crystal surface. Approximately 5 mg of each sample was utilized for spectral acquisition, while plant fibers and seed coat fragments were analyzed directly without additional preparation. The measurements were carried out using a Bruker Alpha II spectrometer equipped with a single-reflection diamond ATR accessory (Bruker Optics GmbH & Co. KG, Ettlingen, Germany), operated via Opus software, at the Research Center for the Conservation of Cultural Property, Fatih Sultan Mehmet Vakıf University. Spectra were recorded in ATR mode, using 96 scans per sample at a resolution of 4 cm^{-1}, to enhance the signal-to-noise ratio. An air spectrum served as the background for each measurement, and data were collected within the mid-infrared range of 4000–400 cm^{-1}. Baseline correction and peak assignments were subsequently performed using dedicated data-processing software (OPUS software, version 8.1, Bruker Optics GmbH & Co. KG, Ettlingen, Germany). Surface smears were taken from pottery, bowls, and jar fragments excavated from the site, with 30 spectra collected per sample group. To improve the detection of organic residues, a chemical extraction was applied to selected samples, after which an additional set of 30 spectra was acquired from the liquid phase of three representative specimens. Prior to ATR-FTIR analysis, selected archaeological samples were subjected to a simple chemical extraction in order to reduce mineral interference and facilitate the characterization of organic functional groups. Each sample was immersed in 100 mL of absolute ethanol and continuously stirred for 1 h at room temperature using a magnetic stirrer (MS-H-Pro+, DLAB Scientific Co., Ltd., Beijing, China). The suspension was subsequently filtered through No. 4 filter paper to remove coarse mineral particles and silicate-rich sediment. The resulting filtrate was allowed to evaporate under ambient laboratory conditions, and the remaining extract was analyzed by ATR-FTIR. This extraction procedure was intended as a sample pre-treatment rather than a selective molecular extraction protocol. Prior to measurement, silicate materials were removed by filtration to isolate the organic-soluble fraction. Furthermore, plant fibers isolated from hearth soils, as well as seeds and a fragment of seed coat retrieved from the same context, were subjected to the same ATR-FTIR measurement protocol. This multi-faceted analytical approach was designed to facilitate the detailed identification of organic residues and to elucidate the compositional characteristics of the archaeological finds with high specificity. Because the archaeological assemblage consisted of a limited number of unique specimens recovered from different archaeological contexts and exhibiting variable preservation states, the FTIR data were evaluated primarily through comparative interpretation of characteristic absorption bands rather than by multivariate statistical analysis. The analytical approach was therefore designed to identify compositional similarities and differences among the archaeological materials instead of establishing statistically significant groupings. To improve analytical reproducibility, multiple spectra were acquired from each sample group under identical instrumental conditions. The repeated measurements were used to verify the consistency of the characteristic absorption bands and to minimize potential variability associated with heterogeneous archaeological materials.

The 30 spectra reported for each sample group represent technical spectral acquisitions obtained from different measurement points within the same archaeological material

category and were acquired to evaluate spectral consistency and reduce the influence of local surface heterogeneity. These spectra should not be interpreted as independent archaeological specimens or biological replicates. Spectral interpretation was based on the reproducibility of the principal absorption bands observed across the repeated measurements rather than on statistical averaging. Independent archaeological specimens are described separately according to their archaeological context and sample category.

2.2. SEM-BSE Imaging

Scanning Electron Microscopy (SEM) imaging was performed to investigate the morphological structure of plant fibers and a seed coat fragment separated from the hearth soil of the excavation site. To enhance conductivity, the samples were mounted onto stubs using carbon tape. Backscattered electron (BSE) images were acquired without applying any additional conductive coating to prevent charging artifacts. The observations were carried out using a Hitachi SU3500 SEM (Hitachi High-Tech Corporation, Tokyo, Japan) instrument equipped with an Oxford X-ACT microanalytical EDX system, operated at the Aluminum Testing, Training and Research Center of Fatih Sultan Mehmet Vakıf University. The SEM measurements were conducted at an accelerating voltage of 15 kV, with a beam current of 140 μA, under a low-vacuum mode maintained at 30 Pa. The analysis focused on capturing the surface texture and morphological features of the fibers and the seed coat without performing elemental analysis.

No chemical conservation treatments were applied to the archaeological materials prior to analysis. Samples were handled using clean laboratory procedures and individually prepared to minimize cross-contamination during analytical measurements. Because the present study was designed as a preliminary multi-analytical characterization of unique archaeological materials, procedural blanks, extraction blanks, and modern reference materials were not included. Consequently, the interpretations presented here should be evaluated within the scope and limitations of the applied analytical protocol.

3. Results and Discussion

3.1. Micromorphological Observations and SEM-BSE Imaging

3.1.1. Fibers and Seed Coat

Fiber and seed coat samples recovered from the archaeological soil matrix were examined under a stereomicroscope in order to determine their micromorphological characteristics (Figure 3). Among the analyzed specimens, Fiber 1 exhibited a homogeneous brown coloration, was well-preserved, and displayed a twisted structure with moderately distinct surface striations. These features are comparable to those reported for several bast-fiber-producing plants described in the archaeobotanical literature. However, these characteristics should be regarded only as comparative morphological indicators and are not sufficient for taxonomic assignment at species level [23,24]. Fiber 5 exhibits angular fractures and possesses a harder morphology with reddish-brown tones. The surface coloration is considered to have possibly resulted from contact with natural pigments or resinous substances [25].

Fiber 8 displays a longer and slightly twisted form, with a clear distinction between inner and outer surfaces. These features are characteristic of well-preserved bast fibers and show a high degree of morphological similarity to bast fibers reported for cultivated fiber plants in the archaeobotanical literature [26]. In contrast, Fibers 4 and 7 exhibit more degraded structures. Fiber 4 presents a transitional coloration between brown and gray with a fragmented texture, whereas Fiber 7 is light-colored, fine in structure, and has smooth edges. These fibers are interpreted as partially degraded bast-like plant fibers. Their morphology may overlap with several fiber-producing taxa; therefore, no reliable

species-level attribution can be made [27,28]. The dark-colored specimen identified as a charred fiber exhibits a hard and brittle structure, distinguished by its carbonized surface. These characteristics indicate that the fiber was exposed to high heat or fire and underwent structural carbonization. Finally, the fragment identified as a seed coat is glossy and reddish-brown in color, with an inclined surface and thick edges. Its bilaterally symmetrical form and dense texture exhibit similarities to seed coats reported for several hard-coated bast-fiber plants, including *Cannabis* spp. However, these similarities should be regarded as comparative observations rather than evidence for taxonomic identification [29–31]. These micromorphological examinations support the interpretation that the examined remains most likely represent bast-like plant tissues showing variable states of preservation and that their states of preservation, degradation, or thermal alteration vary considerably.



Figure 3. Preserved fiber samples (1, 4, 5, 7, and 8) distinguished from the soil matrix of the hearth and ash storage area, together with a charred fiber sample and an intact seed coat.

3.1.2. Charred Seeds

Carbonized seed remains separated from the soil samples of the hearth area in the excavation site were morphologically examined under a stereomicroscope (Figure 4). The seeds generally display colors ranging from dark brown to black and exhibit clear traces of carbonization.

Morphologically, most specimens are oval or ellipsoidal in form, with slightly pointed ends, matte and brittle surfaces, and average lengths ranging between 4 and 7 mm. In some examples, fine striated or granular surface patterns of the seed coat are partially preserved. Additionally, shrinkage of the outer coat, collapse of the inner structure, and other deformations resulting from the burning process were observed. The charred seeds exhibit oval to ellipsoidal morphologies, faint surface ornamentation, and shrinkage features resulting from carbonization. These traits are comparable to those reported for seeds of bast fiber plants in the archaeobotanical literature. However, carbonization substantially alters seed morphology, limiting reliable taxonomic identification [32]. The morphological

shrinkage and fissures in the seed coat caused by carbonization have likewise been reported in previous studies on archaeological seed remains [33].



Figure 4. Charred seeds recovered from the soil of the hearth area of the excavation site.

3.1.3. BSE Imaging of Soil-Extracted Fibers

The BSE images of plant fibers separated from the soil samples at the excavation site provide noteworthy findings regarding microstructural preservation and morphological characteristics. The general view at low magnification (upper left) reveals that the fibers are irregularly distributed within the matrix together with other organic remains, while high-magnification detail images (right and lower frames) show that the cellular structures of the fibers are largely preserved (Figure 5). These microstructures, characterized by thin cell walls, hollow fiber channels, and porous tissues, indicate the presence of xylem-like conductive tissues. Such morphological features are consistent with lignocellulosic bast-like fibers described in archaeobotanical studies but remain insufficient for definitive species discrimination [34].

The presence of surface particles and mineral residues indicates that these fibers show evidence of partial mineral impregnation over time through interaction with minerals in the soil. This suggests either natural preservation of the fibers or the formation of a "possible pseudomorphic preservation" structure in which the organic content was replaced by inorganic elements. A similar preservation scenario was examined by Chen, Jakes, and Foreman (1998), who demonstrated that such fibers can be preserved in a mineralized state under SEM while retaining their internal cellular structures [34]. In addition, the planar parallel striations and smooth fiber surfaces observed in the cross-sections suggest that these fibers may have originated from bast fibers (soft tissues located near the plant bark). Such features are characteristic of natural fiber types commonly encountered in archaeological textile materials and used in yarn production [35]. Such fibers were widely used in ancient textile production, and SEM analyses provide valuable information on fiber morphology and preservation but are insufficient for definitive species-level identification and the determination of their intended use [36]. The plant fibers shown in this image provide strong evidence for archaeobotanical analysis, both in terms of the preservation of their natural structures and their mineralization characteristics. These observations provide evidence for the preservation of plant-derived tissues under complex burial conditions and illustrate the combined effects of carbonization, degradation, and partial mineral impregnation on the archaeological fibers. The observed fiber morphology is compatible

with materials that could have been used in a variety of technological activities, including cordage or textile production. However, the available evidence does not allow confident functional attribution, thereby allowing indirect yet compelling inferences to be drawn regarding the daily practices and technological knowledge at the excavation site.

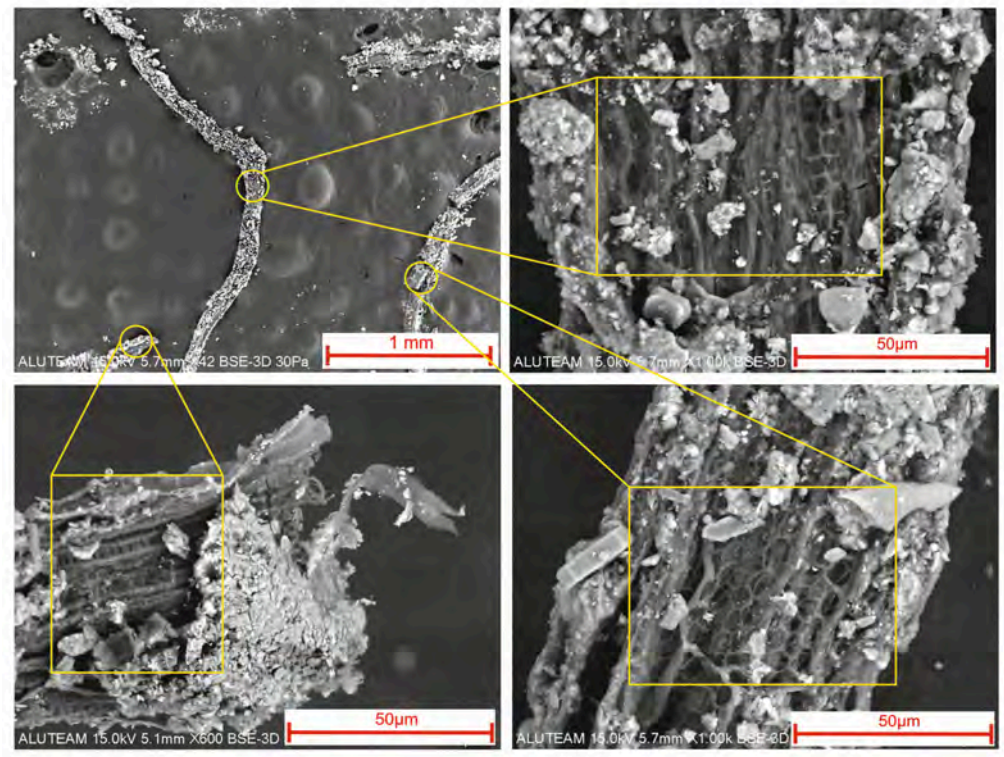


Figure 5. SEM-BSE images of plant fibers.

BSE images of another group of plant fibers, recovered from the same mound excavation but exhibiting clear morphological differences from the previous sample, are presented in Figure 6. The structures in these images are particularly notable for their more regular, parallel fiber bundles and more pronounced longitudinal channels. The elongated, linear patterns and voids observed in the upper right and lower right images suggest that these fibers exhibit morphological variability that may reflect differences in plant source, preservation, or processing history or underwent distinct processing techniques (Figure 6). In particular, the upper right image shows fibers closely aligned and arranged in parallel, which may represent traces of retting or mechanical processing commonly encountered in fibers used for textile production. The degraded and fragmented structure visible in the lower left frame indicates that these fibers were more heavily exposed to environmental factors such as moisture, mineralization, or microbial activity (Figure 6). In addition, the presence of particle residues and irregular mineral deposits on the fiber surfaces suggests that these specimens underwent chemical alteration, or that the organic structures were replaced by inorganic components a type of mineralization process that has been documented in the literature [34]. It may also be considered that this sample is more heavily carbonized or that it belongs to woody tissue rather than bast fibers. Morphological indicators supporting this hypothesis include thick cell walls, fewer voids between the fibers, and smaller, more irregular microscopic channels. Similar structures have been reported in charred fiber specimens by [37]. In addition, variations in fiber structure provide clues about the functional contexts in which they were used. For example, the straight fiber morphology and regular parallel arrangement suggest that these fibers may have been employed in cords, ropes, or woven-based structures. These observations demonstrate that

SEM analyses offer insights not only for species identification but also for understanding functional purposes and levels of technological development [36].

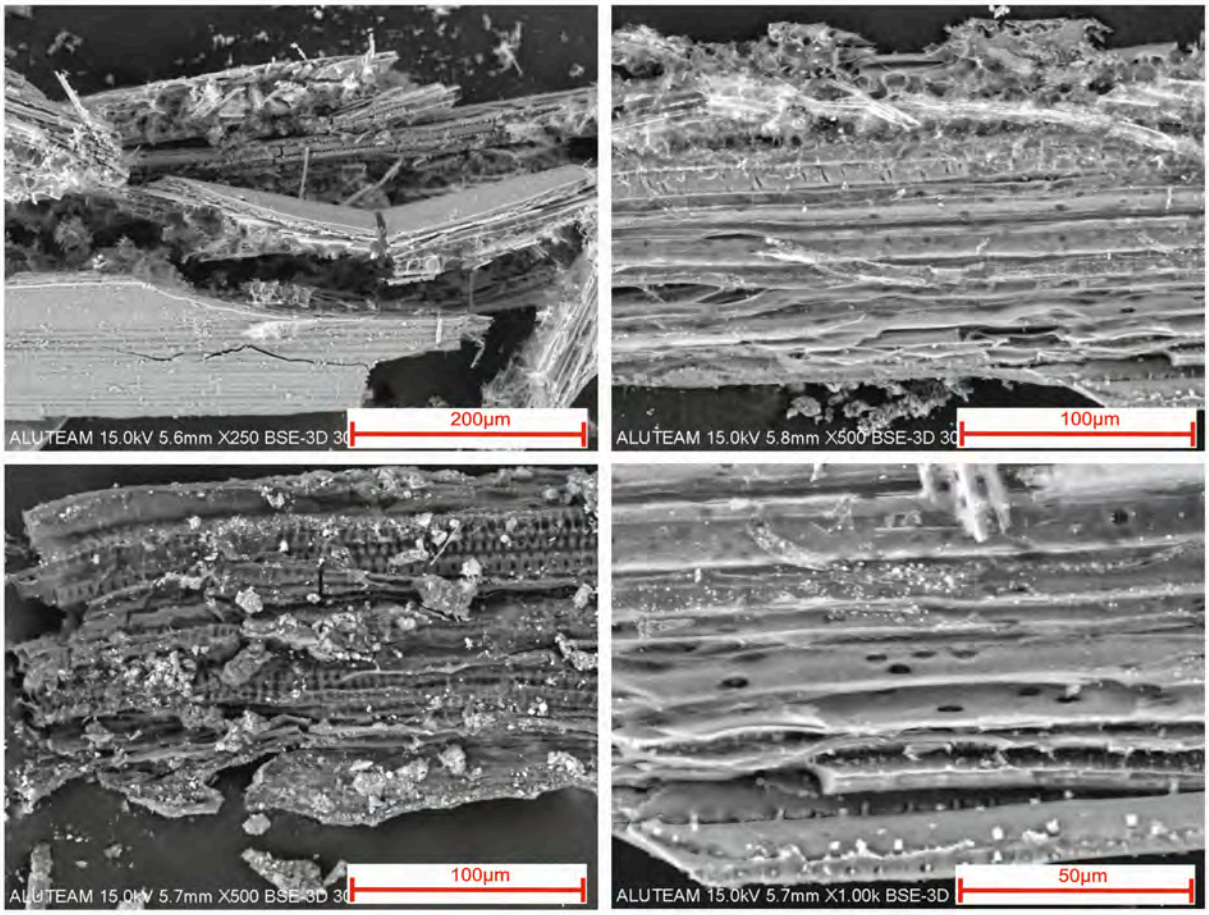


Figure 6. BSE images of a different group of fibers recovered from the same excavation area.

In summary, the fibers in this image display a more regular, denser, and more extensively processed morphology compared to the previous sample. This difference may be related not only to the plant species used but also to the methods of fiber processing, intended function, and the chemical/physical alterations undergone post-burial. These findings suggest the presence of multiple fiber sources at the mound and their use for different purposes, thereby providing important evidence for the technological diversity of the period.

In this SEM-BSE image, the micromorphological structures of a seed coat recovered from the mound excavation are shown in detail (Figure 7). The image on the left reveals a broad, fragmented seed coat surface, while the higher-magnification image on the right exposes fine linear surface patterns and potential microscopic seed coat textures. The observed features are consistent with the morphology of hard seed coats that typically contain sclerenchyma tissue. The cracked and laminar appearance of the surface may have resulted from mechanical stresses following desiccation or from post-burial physical degradation. Such seed coats generally display smooth, slightly raised micromorphological surfaces, with the outer layer exhibiting microscopic striations, granular textures, and fissures [32–38]. Some of these features can be observed in the present image, particularly the fine longitudinal striations in the right frame, which resemble surface morphologies reported for some hard-coated seeds, including *Cannabis* spp.; however, these features are not unique and may also occur in other taxa (Figure 7).

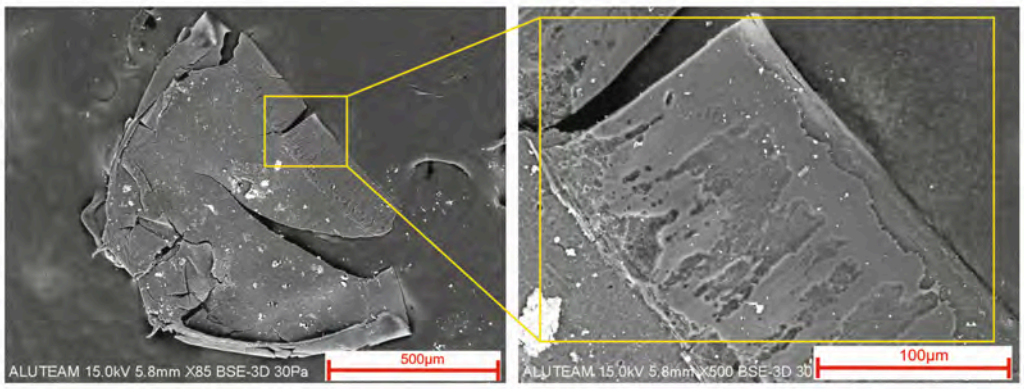


Figure 7. BSE image of an intact seed coat (unburned).

However, as noted in studies such as [29,39], one of the most critical features to consider in the SEM-based identification of Cannabis seed coats is the layered structure of the epidermal cells on the outer surface, which often exhibit lens-like shapes. While the surface morphology observed in these images partially corresponds to these characteristics, a definitive identification requires micromorphological comparison with modern reference samples (such as reference collections or herbarium specimens) [40].

The observed seed coat morphology shares several characteristics with hard-coated seeds described for bast-fiber-producing taxa, including members of the genus Cannabis. Nevertheless, these similarities should be interpreted cautiously because comparable micromorphological features may occur in different taxa, particularly after burial-related alteration and carbonization. Consequently, SEM observations alone cannot support definitive taxonomic identification and should instead be considered as comparative morphological evidence. Reliable species-level attribution would require direct comparison with modern reference collections, together with complementary biomolecular or phytochemical analyses. Especially in the case of ancient seed remains, when such SEM-based investigations prove insufficient, more advanced analytical approaches are required to enable taxonomic identification and to trace historical evidence of agricultural production, such as GC–MS or LC–MS analyses. Such caution is particularly warranted given the effects of carbonization and post-depositional alteration on seed coat microstructures.

The preservation state of the investigated plant-derived remains is most likely the result of multiple post-depositional processes acting simultaneously within the archaeological environment. Carbonization probably contributed to the stabilization of the original plant tissues by increasing their resistance to biological degradation, whereas prolonged burial promoted partial mineral impregnation of the remaining cellular framework. The mineral particles observed on fiber surfaces in the SEM images are consistent with secondary mineral deposition from the surrounding sediment rather than complete replacement of the original organic tissues. Consequently, the analyzed materials appear to represent different stages of preservation, ranging from relatively well-preserved lignocellulosic tissues to partially carbonized and locally mineralized plant remains. Such variability is expected in archaeological deposits where moisture conditions, burial chemistry, microbial activity, oxygen availability, and thermal exposure differ considerably even within the same archaeological context. Therefore, the preservation of these remains should be interpreted as the result of complex taphonomic processes rather than a single mechanism of degradation or mineralization.

3.2. FTIR Spectral Interpretation

3.2.1. Residue Samples from Ceramic Surfaces

The region-based analysis of the FTIR spectra revealed distinct and significant signals in the bowl sample, indicating the presence of organic residues. Broad and intense absorption bands detected in the 3700–3000 cm^{-1} range (~3523 and ~3397 cm^{-1}) are associated with functional groups involved in hydrogen bonding. These bands correspond particularly to the O–H stretching vibrations of hydroxyl (–OH) groups and/or the N–H stretching vibrations of amino ($–NH_2$) groups. The broad band structure observed in this region suggests not only the presence of physically bound water but also organic molecules such as polysaccharides, starch, and protein residues [41,42]. Rather than relying on individual absorption bands alone, the interpretation was based on the overall distribution and relative consistency of the principal functional groups observed among the different archaeological materials. This comparative approach enabled the evaluation of compositional similarities while acknowledging the limitations imposed by the heterogeneous preservation of the archaeological specimens.

In the bowl sample, a strong peak (~1682 cm^{-1}) observed in the 1750–1600 cm^{-1} range corresponds to the stretching vibration of carbonyl (C=O) groups (Figure 8). This peak is associated with esters (R–COOR′), carboxylic acids (–COOH), and amide I groups in protein structures, and is compatible with lipid-containing organic materials, vegetable oils, or cooked carbohydrate-rich residues [43]. At the same time, this region is also where C=C stretching vibrations of aromatic rings may be observed; however, the spectrum is dominated by C=O features. In the 1300–1000 cm^{-1} range, the bowl spectrum exhibits a clearly defined double band (~1101 and ~1031 cm^{-1}), corresponding to C–O stretching vibrations in alcohols and esters (particularly C–O–C ether linkages), as well as C–N stretching vibrations in nitrogen-containing organic compounds. These findings can be interpreted as chemical markers supporting the presence of plant gums, carbohydrate-rich residue derivatives, and protein residues. This spectral region is also of critical importance for the identification of polysaccharides [44]. The absorption bands observed in all samples within the 900–400 cm^{-1} range are associated with inorganic structures. For example, the ~694–698 cm^{-1} range corresponds to Si–O bending vibrations (silicate minerals, quartz), the ~597–601 cm^{-1} range to Al–O stretching vibrations (aluminosilicates, feldspar), and the ~468–421 cm^{-1} range to the deformation vibration characteristics of clay minerals [45]. This region primarily reflects the mineralogical composition of the ceramic raw material and is of secondary importance to the analysis of organic residues.

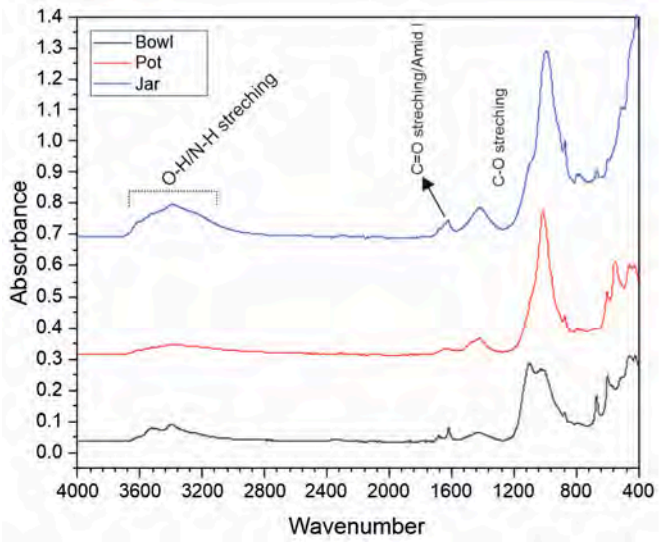


Figure 8. FTIR spectra of ceramic samples (bowl, pot, jar) recovered from the excavation.

Overall, the spectrum of the bowl sample contains strong signals corresponding to the characteristic vibrations of organic functional groups such as O–H, N–H, C=O, C–O, and C–N, providing compelling chemical evidence that the vessel may have come into contact with organic substances in the past (e.g., food, gum, resin). In contrast, the weaker and less intense bands observed in the other samples (pot and jar) suggest that the detection of organic residues in these vessels is less distinct or present at lower concentrations.

3.2.2. Fibers and Seed Coat Fragment

Examination of the ATR-FTIR spectra of fibers recovered from the soil samples revealed characteristic bands associated with cellulose and hemicellulose structures, particularly within the 3600–400 cm^{-1} range (Figure 9). In all samples, the broad band appearing between 3600–3000 cm^{-1} corresponds to O–H stretching vibrations, indicating the hydrophilic nature of the fibers and the presence of polysaccharide structures such as cellulose. This band is especially prominent in Fiber 5 and Fiber 4, whereas it is almost entirely absent in the charred fiber, reflecting the structural degradation of hydroxyl groups due to high-temperature exposure [24,25]. Following this, distinct aliphatic C–H stretching bands were observed at 2921 and 2852 cm^{-1}, most prominently in Fiber 5 but also present in the other samples. These bands correspond to $–CH_2–$ groups and are associated with structures such as cellulose, hemicellulose, and lignin [46]. The markedly reduced signals in these regions in the charred fiber sample indicate the breakdown of the carbon skeleton and partial amorphization of the structure [47].

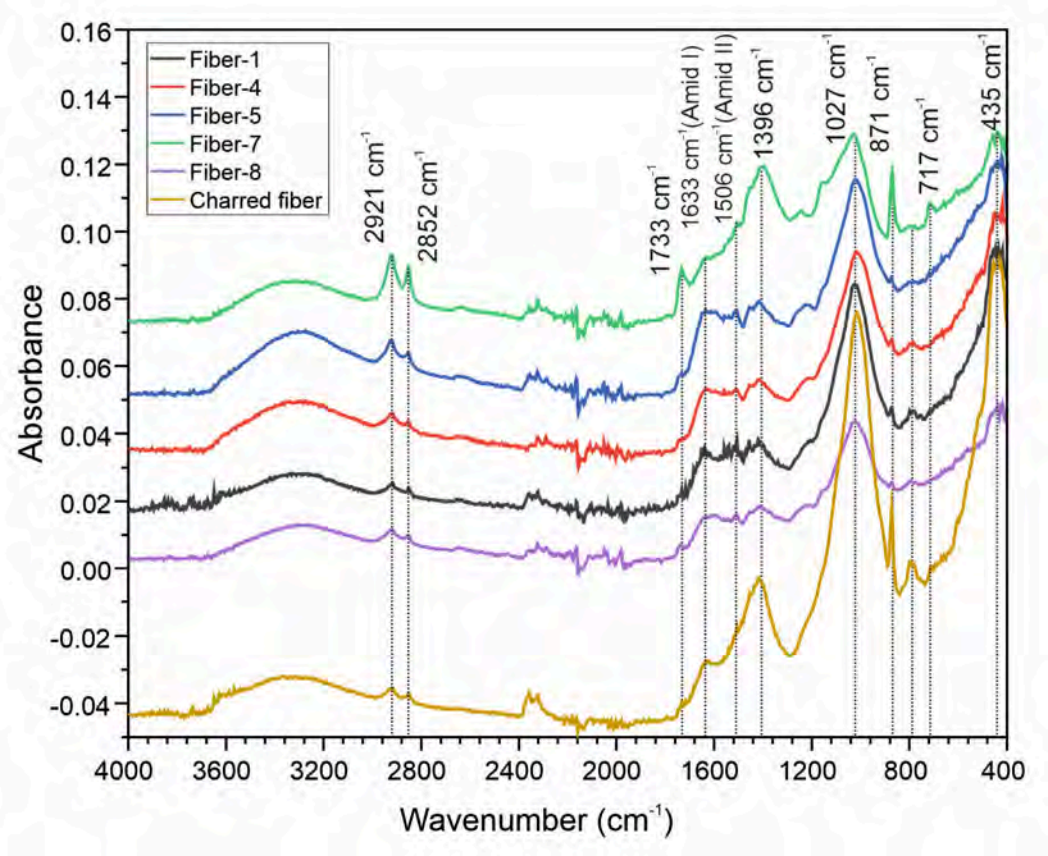


Figure 9. FTIR spectra of fibers distinguished from the soil of the hearth area in the excavation site.

The C=O stretching band detected around 1733 cm^{-1} is particularly prominent in Fiber 5 and Fiber 4. This band is indicative of the acetyl groups of hemicellulose, as well as the presence of pectin and ester linkages [48,49]. In the other samples, this band was observed more weakly, indicating variability in the chemical composition of the fibers. In

the 1650–1500 cm^{-1} region, where the Amide I and Amide II bands occur (particularly at 1633 and 1506 cm^{-1}), low-to-medium-intensity signals were detected in some fiber samples. These bands correspond to protein structures and may indicate small amounts of protein residues naturally present in plant fibers or resulting from environmental contamination [50]. In particular, the prominence of these bands in Fiber 1 and Fiber 5 supports the possibility of surface interactions or the presence of intrinsic nitrogen-containing organic compounds.

The 1396 cm^{-1} band is associated with CH bending and symmetric C–O vibrations. It was observed at moderate intensity in all samples, supporting not only the presence of cellulose structures but also the possible occurrence of carboxylic groups [25]. This band suggests that the original vegetal structures of the fibers are still preserved. In the most characteristic region of the spectrum, between 1200–1000 cm^{-1} (particularly at 1027 cm^{-1}), strong signals corresponding to C–O–C and C–O stretching vibrations were identified in all fibers. This region corresponds to the main structure of cellulose and is strongly preserved in most of the fibers (especially Fiber 5 and Fiber 4). These results indicate that the chemical integrity of the cellulosic framework has been largely maintained [24]. Finally, the "fingerprint" region between 900–400 cm^{-1} represents the part where the greatest differentiation among the fibers is observed. In particular, the bands at 871, 717, and 435 cm^{-1} can be associated with lignin residues, inorganic additives (ash, carbonate), or pyrolysis products. In the charred fiber sample, the broad and amorphous signals observed in this region clearly reflect the structural degradations that occurred as a result of carbonization [47].

ATR-FTIR analyses of Fiber 1 and the seed coat sample recovered from the archaeological excavation site demonstrate that both specimens possess a lignocellulosic structure and share similar functional groups (Figure 10). In the Fiber 1 spectrum, the broad band at ~3277 cm^{-1} corresponds to O–H stretching, the ~2921 and ~2852 cm^{-1} bands to aliphatic C–H stretching vibrations, the ~1740 cm^{-1} band to ester-type C=O stretching, and the bands around ~1513, ~1457, and ~1421 cm^{-1} to aromatic lignin structures. In addition, the distinct absorption observed near ~1022 cm^{-1} reflects C–O stretching vibrations associated with cellulose and hemicellulose structures [25,46,48]. The detected bands correspond to lignocellulosic materials composed primarily of cellulose, hemicellulose, and lignin, which are characteristic of plant-based bast fibers. Similarly, in the seed coat spectrum, broad O–H stretching bands were observed in the ~3743–3600 cm^{-1} range, C–H stretching vibrations in the ~2919 and ~2851 cm^{-1} regions, an ester-related C=O vibration around ~1741 cm^{-1}, and aromatic vibrations derived from lignin at ~1514, ~1453, and ~1423 cm^{-1}. The absorption detected near ~1015 cm^{-1} further indicates that the seed coat contains polysaccharide structures and C–O–C glycosidic linkages [51]. These spectral features demonstrate that the seed coat also possesses a vegetal structure containing lignin, cellulose, and phenolic compounds. Such a biochemical composition is typical of protective plant tissues and is commonly associated with lignocellulosic architectures in seeds. Accordingly, the FTIR spectrum of the seed coat indicates a vegetal lignocellulosic composition with aromatic and carbonyl functional groups, consistent with protective plant seed tissues [52,53].

The similar FTIR spectral features indicate that Fiber 1 and the seed coat share a broadly similar lignocellulosic composition. However, these similarities reflect common structural biopolymers present in many vascular plants and therefore do not permit inference of a shared botanical origin or species-level relationship. Because cellulose, hemicellulose, lignin, and their associated functional groups are widely distributed among lignocellulosic plants, FTIR spectroscopy primarily provides compositional information and should not be used alone to infer common botanical origin or species identity. Consequently, the

FTIR results should be interpreted as evidence of compositional similarity rather than taxonomic affinity.

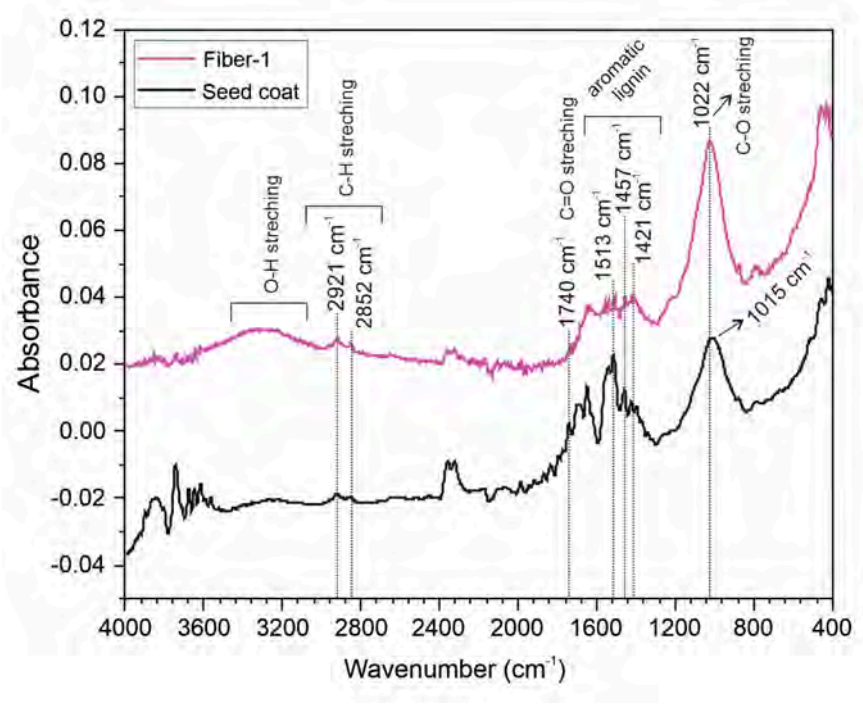


Figure 10. Comparison of seed coat and fiber spectra from the hearth-area soil of the excavation site.

The absorptions observed in the low-frequency region of the spectrum (420–800 cm^{-1}) may be associated with inorganic phases formed during the mineralization of plant remains or with soil-derived contributions [45].

3.3. TG Thermograms

Thermogravimetric analysis (TG) and derivative thermogravimetry (DTG) were applied to evaluate the thermal decomposition behavior and potential organic matter content in soil smear residues sampled from the surfaces of three ceramic objects excavated from an archaeological context: a bowl, a jar, and a pot. The mass loss events observed during the heating program from ambient temperature to 1000 °C provided valuable insights into both inorganic (e.g., carbonate) and organic (e.g., biogenic residues) content.

3.3.1. Bowl Sample

The TG and DTG curves of the bowl sample clearly display distinct mass loss steps during the heating program between 25 °C and 1000 °C (Figure 11). The first noticeable mass loss is associated with weak DTG peaks observed at 72 °C and 133 °C. The mass loss of approximately 6–7% within this temperature range is primarily attributed to the removal of free or hygroscopic water present in the sample. Some studies have noted that pronounced mass losses in this region are observed in ceramics that underwent post-burial rehydration [54,55]. The DTG peak appearing around 321 °C is thought to indicate the decomposition of organic residues and possible biogenic remains. It may also be associated with the combustion of organic additives incorporated into the clay paste prior to firing. Such organic degradations are commonly observed within the 250–400 °C range [56,57].

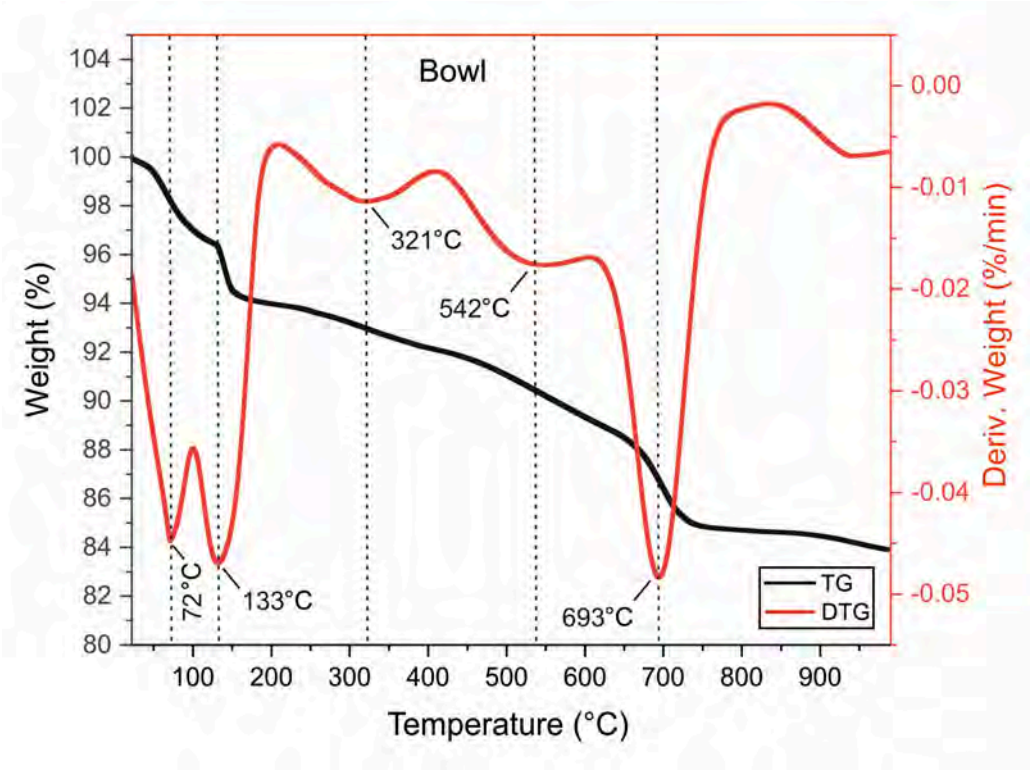


Figure 11. TG and DTG curves of the bowl sample.

The pronounced mass loss at 542 °C is most likely associated with the dehydroxylation of clay minerals [55]. Finally, the sharp mass loss and DTG peak observed around 693 °C indicate the decomposition of carbonates, particularly calcite. The mass loss in this region suggests that the firing temperature of the sample was below 750 °C. A research team has demonstrated that firing temperatures below 700 °C prevent the complete decomposition of carbonates [58]. Overall, the TG/DTG data obtained for the bowl sample indicate a multi-stage thermal decomposition process, involving different forms of bound water, residual organic compounds, and carbonate content at high temperatures.

3.3.2. Jar Sample

Similarly, in the jar sample, the first mass loss is defined by DTG peaks observed at 65 °C and 132 °C (Figure 12). The mass loss in this temperature range (~6–7%) is generally attributed to the evaporation of free (physically bound) water retained on the surface or within the pore structure. As in the bowl sample, the occurrence of a double water-loss event indicates that the specimen was subjected to a rehydration process [55]. The additional DTG peaks observed around 190 °C and 307 °C indicate the sequential decomposition of possible organic residues, biogenic remains, or humic substances introduced from the burial environment. In ancient ceramics, it has been noted that pre-firing additives (such as plant fibers, oils, or resins) typically degrade within this temperature range [57,58].

The pronounced mass loss at 521 °C is associated with the dehydroxylation of clay minerals. This process has been linked to the early vitrification stage of the ceramic [59]. The sharp peak observed around 695 °C indicates the thermal decomposition of carbonate phases, particularly calcite. This decomposition step suggests that the firing temperature may have occurred around 690–720 °C, a range that has been described in the literature as "low-temperature firing" [56]. In conclusion, the jar sample exhibits a multi-step thermal decomposition mechanism, indicating the presence of free water, organic residues, clay minerals, and carbonate contents.

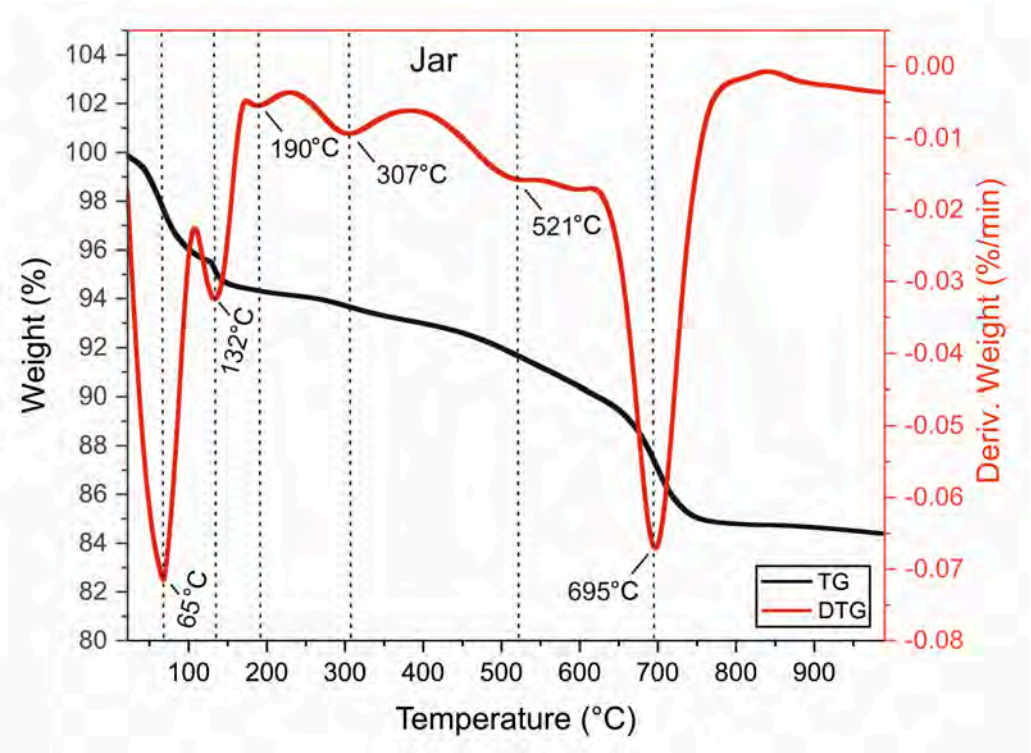


Figure 12. TG and DTG curves of the jar sample.

3.3.3. Pot Sample

According to the TG curve (black), the sample experienced a total mass loss of approximately 18%. The DTG curve (red) indicates four distinct mass loss peaks at 72 °C, 321 °C, 490 °C, and 713 °C (Figure 13). The first mass loss occurs around 72 °C and is associated with the removal of physically adsorbed surface moisture and hygroscopic water within the porous ceramic matrix. The second and third mass losses, occurring at 321 °C and 490 °C, respectively, represent a double organic decomposition peak, potentially reflecting the presence of both natural organics and organic matter introduced during the burial process after firing. Such double organic decomposition curves have been associated with high-organic-content Neolithic samples [56]. These organics may represent biogenic substances and humic acids adsorbed onto the ceramic surface during the burial process or organic contaminants related to the ancient use of the vessel.

The most pronounced mass loss occurred at 713 °C. This temperature corresponds to the decomposition zone of calcium carbonate ($CaCO_3$), where it breaks down into calcium oxide (CaO) and carbon dioxide (CO_2) [57,58]. This suggests that the sample was fired at a temperature (~720 °C) where complete decomposition did not occur. Such firing temperatures have been widely documented in traditional firing techniques [57]. The absence of significant mass loss above 713 °C indicates that the initial firing temperature of the ceramic did not exceed this threshold, suggesting production within a low-to-medium-temperature firing regime (~700–750 °C). This phenomenon is frequently observed, particularly in handmade prehistoric and early historic ceramics [60].

It should be noted that the TG/DTG data provide only approximate information regarding the thermal history of the analyzed archaeological materials. Carbonate decomposition temperatures may be influenced by several factors, including burial-related alteration, mineralogical composition, particle size, heating conditions, and post-depositional calcite precipitation. Therefore, the thermal behavior observed in this study is interpreted as comparative evidence of thermal exposure rather than a precise determination of the original firing temperature.

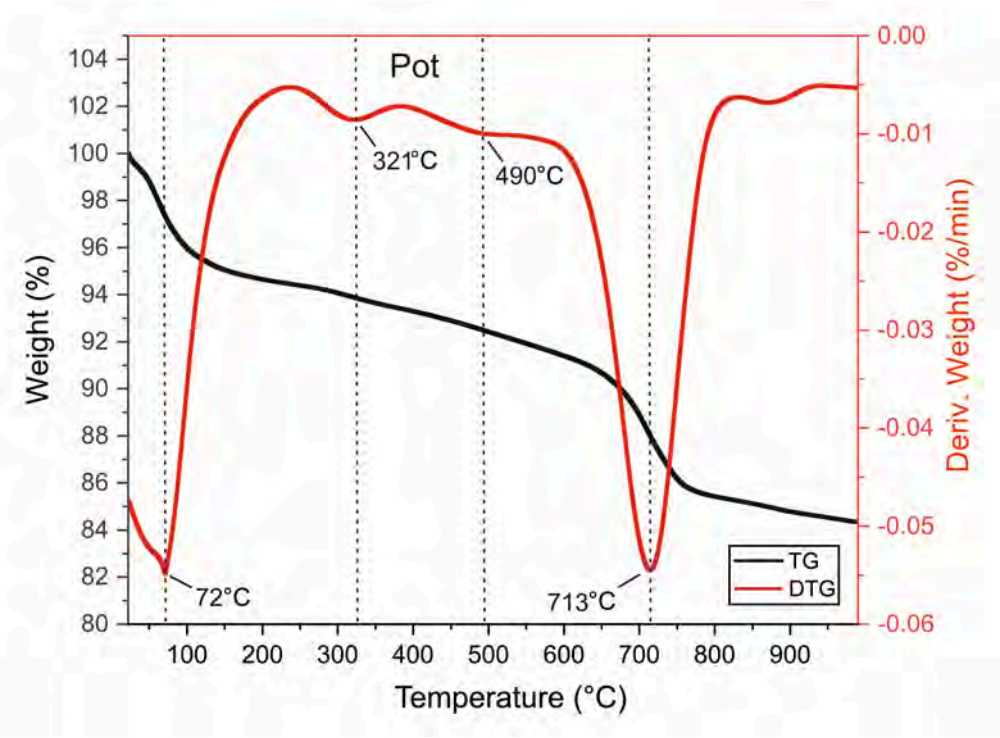


Figure 13. TG and DTG curves of the pot sample.

3.4. Comparative Evaluation of Organic Matter Content

Based on the DTG responses, all three samples exhibit low-temperature peaks indicative of physically bound water yet differ in organic matter preservation. The pot sample displays the strongest organic signal, with two distinct DTG peaks (321 °C and 490 °C), suggesting well-preserved carbonized residues. The bowl shows a moderate signal at 321 °C, while the jar exhibits a mild response around 190–307 °C, indicating limited organic content or partial degradation. Carbonate decomposition is observed in all samples around 690–713 °C, with varying intensities. The bowl shows the most pronounced carbonate loss, implying a higher $CaCO_3$ content or better preservation. The pot and jar display moderate to low intensities, suggesting differences in raw material or firing atmosphere. Overall, these variations reflect distinct firing conditions, clay compositions, and post-depositional histories. A summary of the thermogravimetric responses and corresponding interpretations for each sample is presented in Table 2.

Table 2. Comparative DTG Parameters for Organic and Carbonate Decomposition.

Sample	Low-Temp DTG Peak (<200 °C)	Organic Matter Signal	Carbonate Decomp. Temp (°C)	Intensity of Carbonate Peak
Bowl	72, 133 °C	Moderate (321 °C)	693 °C	Moderate–High
Jar	65, 132 °C	Mild (190, 307 °C)	695 °C	Low–Moderate
Pot	72 °C	Strong (321, 490 °C)	713 °C	Moderate

The thermal behavior of the analyzed samples was evaluated through comparison of the principal decomposition intervals and DTG peak positions. Although these thermal characteristics provide useful comparative information, they should be regarded as semi-quantitative indicators rather than precise measurements of firing conditions because post-depositional alteration and sample heterogeneity may influence thermal responses.

3.5. Regional Similarities in Archaeological Fiber Remains: A Comparative Assessment with Anatolian Examples

Archaeological excavations carried out at various mounds in Anatolia have revealed findings that date fiber production and use to very early periods. Direct and indirect remains of plant-based fibers, particularly flax (Linum usitatissimum) and hemp (Cannabis sativa), indicate the continuity of textile production in Anatolia from the Neolithic to the Late Bronze Age. For example, at Çatalhöyük in Konya, carbonized textile fragments dating to around 6000 BCE have been identified. These examples were produced using the plain weave technique, and the material is thought to have been wool or flax [61]. Similarly, flax fibers dating to the Neolithic period have been identified in the excavations at Çayönü in Diyarbakır, demonstrating that early farming communities possessed knowledge of weaving technology [61].

In the samples dated to the Chalcolithic and Bronze Ages, indirect evidence of textile production has been identified. At Gülpınar Höyük in Çanakkale, the discovery of spindle whorls, loom weights, and pottery sherds bearing impressions of woven fabrics indicates the presence of fiber-processing and weaving activities at the settlement [61]. At Tepecik Höyük, loom weights dated to the Late Bronze Age provide further evidence supporting the continuity of local textile production in western Anatolia [62]. Archaeobotanical analyses likewise document the presence of diverse plants remaining across Anatolia. For example, studies conducted at Barcın Höyük have identified carbonized seed remains dating to 6600–6300 BCE, offering insights into early agricultural practices and plant utilization [63]. In addition, organic residue analyses of pottery from western Anatolia and the Marmara region have revealed plant- and animal-derived lipids, together with traces of use-related residues [64]. In light of these data, the fiber and seed coat-like remains recovered from Oluz Höyük are considered to be consistent with plant-based materials such as flax and hemp, and with long-standing fiber-processing traditions in Anatolia extending back to the Neolithic period.

These observations may be discussed within a broader Near Eastern framework of plant use. In this context, independent evidence from the Judahite shrine at Tel Arad demonstrates the deliberate ritual use of Cannabis sativa, as shown by the identification of cannabinoids (THC, CBD, and CBN) on Iron Age altars [65]. While such direct chemical evidence is absent at Oluz Höyük and species-level identification cannot be established, the presence of bast-fiber plant remains in ritualized contexts invites cautious comparison with wider Near Eastern traditions of plant use in cultic practices.

Despite these observations, important methodological constraints must be acknowledged. We emphasize that the analytical protocol applied here (SEM-BSE, ATR-FTIR, TG/DTG) does not provide species-level resolution. Accordingly, the taxonomic discussion is restricted to broad bast-fiber categories, and references to hemp or flax should be understood as plausible analogues rather than definitive identifications. Future work integrating GC-MS/Py-GC-MS and DNA-based approaches will be required to test these hypotheses more rigorously.

The analytical workflow applied in this study successfully demonstrates the value of combining stereomicroscopy, SEM-BSE, ATR-FTIR, and TG/DTG for the characterization of archaeological plant-derived remains. Nevertheless, these methods primarily provide morphological and compositional evidence and should not be interpreted as definitive tools for species-level taxonomic identification. Future studies integrating modern comparative reference collections, morphometric analyses, biomolecular approaches (e.g., ancient DNA), and targeted biomarker analyses will be essential for confirming botanical identity with greater confidence.

The FTIR and TG/DTG datasets were interpreted using a comparative analytical framework based on the relative distribution of characteristic spectral bands and thermal events across the investigated archaeological materials. Because the analyzed specimens represent unique archaeological finds recovered from different depositional contexts and exhibiting varying degrees of preservation, statistical treatment was considered inappropriate for the present dataset. Nevertheless, the consistency observed among the principal spectral and thermal features provides robust comparative evidence supporting the compositional interpretations presented in this study.

4. Conclusions

This study presents a comprehensive archaeometric assessment of plant-derived organic remains, particularly bast fibers and seed coats recovered from the archaeological site of Oluz Höyük. By employing complementary methods such as stereomicroscopic examination, SEM-BSE imaging, ATR-FTIR spectroscopy, and TG (thermogravimetric analysis), the research has provided significant micromorphological, chemical, and thermal evidence revealing possible organic residues in ancient ceramics, the presence and preservation state of ancient fiber materials, and their potential botanical origins.

The main findings of this study can be summarized as follows:

- Micromorphological and BSE analyses revealed the presence of various plant fibers, most of which were well preserved and exhibited diagnostic features of bast fibers, such as striations, hollow channels, and fiber bundles. In particular, Fiber 1 and Fiber 8 share morphological traits reported for bast fibers of cultivated fiber plants (e.g., hemp or flax), although these features are not sufficient for definitive species-level identification. More degraded structures observed in other fibers may reflect either different bast-fiber taxa or post-burial alteration processes.
- SEM-BSE imaging of the fibers and seed coats revealed a high degree of microstructural preservation, including identifiable cell walls, lumen channels, and fiber bundles, together with partial mineralization. This preservation state supports archaeobotanical interpretation of the remains while highlighting mineral-mediated stabilization processes acting during burial.
- ATR-FTIR spectra revealed characteristic O–H, C–H, C=O, and C–O–C vibration bands indicating the presence of cellulose and lignin structures. The overlapping spectral features observed in both fiber and seed coat samples point to a common botanical origin. By contrast, in the charred fiber, these bands were markedly reduced, reflecting structural degradation caused by thermal alteration.
- TG and DTG analyses of ancient ceramic samples provided significant insights into production processes and post-use alterations. In all samples, low-temperature mass losses (~65–133 °C) indicated the removal of free and hygroscopic water, likely related to the porous matrix and post-burial rehydration. In terms of organic matter degradation, the pot sample exhibited the strongest signal with a distinct double peak at 321 °C and 490 °C, suggesting good preservation of carbonized organic residues. The bowl sample presented a moderate signal at 321 °C, whereas the jar sample displayed only weak organic reactions between 190 and 307 °C. These differences may be related to variations in raw material composition, use practices, or burial conditions. Carbonate decomposition peaks were observed in all three samples within the 690–713 °C range. The most pronounced decomposition occurred in the bowl sample, suggesting either a higher calcite content or a more efficient decomposition process. Overall, these findings indicate that the vessels were produced at similar firing temperatures (~690–720 °C), while differences in raw materials and environmental conditions influenced their thermal responses.

Taken together, comparable chemical fingerprints observed in fibers and seed coat fragments indicate a shared lignocellulosic plant origin, consistent with bast-fiber plant use at the site. When integrated with micromorphological observations, these data suggest intentional exploitation of plant fibers while precluding definitive species-level identification.

The analytical interpretations presented here should therefore be regarded as comparative and semi-quantitative rather than fully quantitative assessments, reflecting the inherent limitations associated with heterogeneous archaeological organic remains.

All of these findings not only confirm the archaeologically significant presence of bast fibers and seed structures at Oluz Höyük but also provide detailed data on their preservation states and chemical characteristics. Furthermore, comparisons with Neolithic and Chalcolithic centers in Anatolia point to the historical continuity of plant fiber use, particularly flax and hemp.

Archaeological findings from Oluz Höyük are noteworthy in terms of fiber technologies, preservation of plant-based residues, and their broader cultural implications. The combined micromorphological (stereomicroscopy, SEM-BSE) and spectroscopic (ATR-FTIR) data indicate that the recovered fibers and seed coat fragments originate from bast-fiber plants. Their morphological traits are comparable to those reported for cultivated fiber taxa such as hemp (Cannabis sativa) and flax (Linum usitatissimum); however, the available evidence does not allow for definitive species-level identification. Accordingly, Cannabis sativa should be regarded as a plausible reference taxon rather than a demonstrated botanical identification. Within a broader Near Eastern context, independent evidence from sites such as Tel Arad demonstrates the deliberate ritual use of Cannabis sativa, supported by direct chemical identification of cannabinoids on Iron Age altars. Although the archaeological context at Oluz Höyük is compatible with ritual activities, the present study did not include cannabinoid detection or cannabis-specific biomolecular analyses. Therefore, no direct evidence for ritual cannabis use can be inferred from the analytical data presented here. Consequently, the comparison with Tel Arad is intended only to provide broader archaeological context, and any possible association with ritual plant use at Oluz Höyük should be regarded solely as a contextual archaeological hypothesis rather than as a conclusion supported by chemical evidence.

Author Contributions: İ.C. contributed to the investigation and writing of the manuscript. E.K. contributed to the conceptualization of the study, investigation, data analysis, manuscript writing, critical review and editing, and supervised the overall research process. Ş.D. contributed to the investigation, manuscript writing, and supervision. M.S. contributed to the investigation and manuscript writing. All authors have read and agreed to the published version of the manuscript.

Funding: This research received no external funding.

Institutional Review Board Statement: Not applicable.

Informed Consent Statement: Not applicable.

Data Availability Statement: The original contributions presented in the study are included in the article, further inquiries can be directed to the corresponding author.

Acknowledgments: The authors would like to express their sincere gratitude to the entire project team involved in the preparation of the 2024 Excavation Report of Oluz Höyük, which provided valuable contextual support during the writing of this article. We also extend our appreciation to the dedicated staff of the ALUTEAM Laboratory Unit at Fatih Sultan Mehmet Vakıf University for their assistance in carrying out the necessary analytical procedures.

Conflicts of Interest: The authors declare no conflicts of interest.

References

1. Dönmez, Ş. *Amasya-Oluz Höyük: Kaşku Ülkesi'nin Önemli Kenti. 2007 ve 2008 Dönemi Çalışmaları Genel Değerlendirmeler ve ön Sonuçlar/The Principal Site of Kaşku Land: The Preliminary Reports of 2007 and 2008 Seasons General Evaluations and Results*; Governorship of Amasya: Ankara, Türkiye, 2010. [CrossRef]
2. Dönmez, Ş. Oluz Höyük: Kuzey-Orta Anadolu'nun Kralî Pers Merkezi. In *Güneş Karadeniz'den Doğar. Sümer Atasoy Armağanı/Lux Ex Ponto Euxino: Studies Presented in Honour of Sumer Atasoy*; Dönmez, Ş., Ed.; Hel Publications: Ankara, Türkiye, 2013.
3. Dönmez, Ş.; Saba, M. Anadolu Demir Çağı Pers Tarihi ve Oluz Höyük (Kritalla)/Anatolian Iron Age Persian History and Oluz Höyük (Kritalla). In *Orta ve Doğu Anadolu Geç Demir Çağı: Post-Urartu, Med ve Akhaimenid İmparatorlukları/Central and Eastern Anatolia Late Iron Age: Post-Urartu, Median and Achaemenid Empires*; Özfırat, A., Dönmez, Ş., Işıklı, M., Saba, M., Eds.; Ege Yayınları: Istanbul, Turkey, 2019.
4. Dönmez, Ş. *Amasya-Oluz Höyük: Kuzey-Orta Anadolu'da Bir Akhaimenid (Pers) Yerleşmesi. 2009–2013 Çalışmaları Genel Değerlendirmeler ve Önsonuçlar*; Maviay Yayıncılık: Amasya, Türkiye, 2017.
5. Dönmez, Ş. Kuzey-Orta Anadolu'da Yeni Bir Arkeolojik Keşif: Oluz Höyük Kubaba (Matar Kubileya) Tapınağı. In *Arkeoloji İle Geçen Bir Yaşam İçin Yazılar: Veli Sevin'e Armağan/Scripta Essays in Honour of Veli Sevin*; Özfırat, A., Ed.; Ege Yayınları: İstanbul, Türkiye, 2014.
6. Dönmez, Ş. Early Zoroastrianism at Oluz Höyük, North-Central Anatolia. In *Context and Connection: Studies on the Archaeology of the Ancient Near East in Honour of Antonio Sagona*; Batmaz, A., Bedianashvili, G., Michalewicz, A., Robinson, A., Eds.; Peeters Publishers: Leuven, Belgium, 2018.
7. Dönmez, Ş. Oluz Höyük Kazıları Işığında Kuzey-Orta Anadolu (Pontika Kappadokia) Akhaimenid Varlığına Güncel Bir Bakış. *TÜBA-AR Türkiye Bilim. Akad. Arkeol. Derg.* **2015**, *18*, 71–107. [CrossRef]
8. Dönmez, Ş. A New Excavation in Pontic Cappadocia: Amasya-Oluz Höyük. Preliminary Results for the Hellenistic Period and Iron Age Layers. In *The Black Sea, Paphlagonia, Pontus and Phrygia in Antiquity: Aspects of Archaeology and Ancient History*; Tsetskhladze, G., Ed.; British Archaeological Reports: Oxford, UK, 2012.
9. Dönmez, Ş. Oluz Höyük: Preliminary Results for the Hellenistic Period and Iron Age Layers. In *Proceedings of the Fourth International Congress on Black Sea Antiquities, Istanbul, Türkiye, 14–18 September 2009*; Tsetskhladze, G.R., Atasoy, S., Avram, A., Dönmez, Ş., Hargrave, J., Eds.; British Archaeological Reports: Oxford, UK, 2013; pp. 363–371, ISBN 978-605-7673-18-3.
10. Dönmez, Ş. Preliminary Results on the Hellenistic and Iron Age Phases at Oluz Höyük. In *Recent Studies on the Archaeology of Anatolia*; Laflı, E., Patacı, S., Eds.; Archaeopress: Oxford, UK, 2015.
11. Dönmez, Ş. Achaemenid Presence at Oluz Höyük, North-Central Anatolia. In *Proceedings of the Fifth International Congress on Black Sea Antiquities, Belgrade, Serbia, 17–21 September 2013*; Tsetskhladze, G.R., Avram, A., Hargrave, J., Eds.; Archaeopress Publishing: Oxford, UK, 2015; pp. 467–473.
12. Dönmez, Ş. The Contribution of New Research to Hittite Historical Geography of Amasya Province. In *Place and Space in Hittite Anatolia I: Hatti and the East; Proceedings of the International Workshop, İstanbul, Türkiye, 25–26 October 2013*; Türk Eskiçağ Bilimleri Enstitüsü: İstanbul, Turkey, 2017; pp. 75–90.
13. Dönmez, Ş. The Land of Sacred Fire: Amasya–Oluz Höyük. In *Settlement and Necropoleis of the Black Sea and Its Hinterland in Antiquity*; Archaeopress Publishing: Oxford, UK, 2019.
14. Dönmez, Ş. A Punic Necklace from Oluz Höyük: A General Evaluation for Anatolia. In *Proceedings of the Sixth International Congress on Black Sea Antiquities, Constanta, Romania, 18–22 September 2017*; Tsetskhladze, G.R., Avram, A., Hargrave, J., Eds.; Archaeopress Publishing: Oxford, UK, 2021; pp. 400–405.
15. Dönmez, Ş.; Saba, M. New Discoveries at Oluz Höyük: An Early Zoroastrian Sanctuary in North-Central Anatolia. *Archaeol. Anatolia* **2019**, *3*, 112–121.
16. Dönmez, Ş.; Abazoğlu, F. Kızılırmak Havzası Demir Çağı Çanak-Çömlek Geleneğinin Kökeni Üzerine Düşünceler. *TÜBA-AR Türkiye Bilim. Akad. Arkeol. Derg.* **2018**, *23*, 81–99.
17. Dönmez, Ş.; Abdullaev, K. Oluz Höyük–Amasya: Discovery of a Site in the North of Central Anatolia. *J. Anc. Hist.* **2019**, *79*, 703–729. [CrossRef]
18. Dönmez, Ş.; Abazoğlu, F. Hitit Sonrası Kuzey-Orta Anadolu: Oluz Höyük'te Karanlık Çağ ile İlgili Yeni Bulgular. In *Proceedings of the IXth International Congress of Hittitology*; Turkish Corum Governorship, Provincial Directorate of Culture and Tourism Publications: Çorum, Turkey, 2019; pp. 237–260.
19. Dönmez, Ş.; Saba, M. Oluz Höyük: Persian (Akhaimenid) Settlement in North-Central Anatolia. In *Proceedings of ICE1: Identity, Diversity and Contact from the Southern Balkans to Xinjiang, from the Upper Paleolithic to Alexander*; Lebeau, M., Ed.; Brepols Publisher: Turnhout, Belgium; Brussels, Belgium, 2021; pp. 275–296.
20. Dönmez, Ş.; Yurtsever Beyazıt, A. Oluz Höyük: A Multicultural Settlement in Pontic Cappadocia. In *Amasya: Maid of Mountains*; Özdem, F., Ed.; Yapı Kredi Yayınları: İstanbul, Turkey, 2014; pp. 51–71.
21. Dönmez, Ş.; Yurtsever Beyazıt, A. Oluz Höyük 2013 Dönemi Çalışmaları. In *Amasya-Oluz Höyük: Kuzey-Orta Anadolu'da Bir Akhaimenid (Pers) Yerleşmesi. 2009–2013 Çalışmaları Genel Değerlendirmeler ve Önsonuçlar*; Amasya Valiligi: Amasya, Türkiye, 2017.

22. Dönmez, Ş. *Oluz Höyük Kazısı Onsekizinci (2024) Dönem Çalışmaları Değerlendirme Sonuç Raporu*; T.C. Kültür ve Turizm Bakanlığı, Kültür Varlıkları ve Müzeler Genel Müdürlüğü: Altındağ, Turkey, 2024.
23. Venturas, M.D.; Sperry, J.S.; Hacke, U.G. Plant Xylem Hydraulics: What We Understand, Current Research, and Future Challenges. *J. Integr. Plant Biol.* **2017**, *59*, 356–389. [CrossRef] [PubMed]
24. Poletto, M.; Pistor, V.; Zattera, A.J. Structural Characteristics and Thermal Properties of Native Cellulose. In *Cellulose: Fundamental Aspects*; InTech: Rijeka, Croatia, 2013. [CrossRef]
25. Pandey, K.K. A Study of Chemical Structure of Soft and Hardwood and Wood Polymers by FTIR Spectroscopy. *J. Appl. Polym. Sci.* **1999**, *71*, 1969–1975. [CrossRef]
26. Garcia-Jaldon, C.; Dupeyre, D.; Vignon, M.R. Fibres from Semi-Retted Hemp Bundles by Steam Explosion Treatment. *Biomass Bioenergy* **1998**, *14*, 251–260. [CrossRef]
27. Schweingruber, F.H. *Anatomy of European Woods*; Verlag Paul Haupt: Stuttgart, Germany, 1990.
28. Liu, J.; Guo, D.; Zhou, Y.; Wu, Z.; Li, W.; Zhao, F.; Zheng, X. Identification of Ancient Textiles from Yingpan, Xinjiang, by Multiple Analytical Techniques. *J. Archaeol. Sci.* **2011**, *38*, 1763–1770. [CrossRef]
29. Fleming, M.P.; Clarke, R.C. Physical Evidence for the Antiquity of *Cannabis sativa* L. *J. Int. Hemp Assoc.* **1998**, *5*, 80–93. ISSN/ISBN: 1381-091X.
30. Small, E. *The Species Problem in Cannabis: Science and Semantics*; Corpus Information Services: Ottawa, ON, Canada, 1979; Volume 2.
31. Schlumbaum, A.; Tensen, M.; Despres, V.J. Ancient Plant DNA in Archaeobotany. *Veg. Hist. Archaeobot.* **2007**, *17*, 233–244. [CrossRef]
32. Jiang, H.E.; Li, X.; Zhao, Y.X.; Ferguson, D.K.; Hueber, F.; Bera, S.; Wang, Y.F.; Zhao, L.C.; Liu, C.J.; Li, C.S. A New Insight into Cannabis sativa Utilization from 2500-Year-Old Yanghai Tombs, Xinjiang, China. *J. Ethnopharmacol.* **2006**, *108*, 414–422. [CrossRef] [PubMed]
33. Van der Veen, M. Formation Processes of Desiccated and Carbonized Plant Remains: The Identification of Routine Practice. *J. Archaeol. Sci.* **2007**, *34*, 968–990. [CrossRef]
34. Chen, H.L.; Jakes, K.A.; Foreman, D.W. SEM, EDS, and FTIR Examination of Archaeological Mineralized Plant Fibers. *Text. Res. J.* **1996**, *66*, 219–224. [CrossRef]
35. Borojevic, K.; Mountain, R. Microscopic Identification and Sourcing of Ancient Egyptian Plant Fibres Using Longitudinal Thin Sectioning. *Archaeometry* **2013**, *55*, 81–112. [CrossRef]
36. Kallenbach, E. Testing the Feasibility of Fiber Identification for Fine Cordage Artifacts from the Paisley Caves, Oregon. *J. Archaeol. Sci.* **2023**, *158*, 105855. [CrossRef]
37. Srinivasan, R.; Jakes, K.A. Optical and Scanning Electron Microscopic Study of the Effects of Charring on Indian Hemp (*Apocynum cannabinum* L.) Fibres. *J. Archaeol. Sci.* **1997**, *24*, 1137–1147. [CrossRef]
38. Bai, Y.; Jiang, M.; Xie, T.; Jiang, C.; Gu, M.; Zhou, X.; Yan, X.; Yuan, Y.; Huang, L. Archaeobotanical Evidence of the Use of Medicinal Cannabis in a Secular Context Unearthed from South China. *J. Ethnopharmacol.* **2021**, *275*, 114114. [CrossRef] [PubMed]
39. McPartland, J.M.; Hegman, W. *Cannabis* Utilization and Diffusion Patterns in Prehistoric Europe: A Critical Analysis of Archaeological Evidence. *Veg. Hist. Archaeobot.* **2018**, *27*, 627–634. [CrossRef]
40. Waudby, D.B. Critical Evaluation of Techniques for the Identification of Archaeological Bast Fibres: Flax, Hemp and Nettle. Ph.D. Thesis, University of York, York, UK, 2025.
41. Oudemans, T.F.M.; Erhardt, D. Organic Residue Analysis in Ceramic Studies: Implications for Conservation Treatment and Collections Management. *Stud. Conserv.* **1996**, *41*, 137–142. [CrossRef]
42. Lettieri, M. Infrared Spectroscopic Characterization of Residues on Archaeological Pottery through Different Spectra Acquisition Modes. *Vib. Spectrosc.* **2015**, *76*, 48–54. [CrossRef]
43. Colombini, M.P.; Giachi, G.; Modugno, F.; Ribechini, E. Characterisation of Organic Residues in Pottery Vessels of the Roman Age from Antinoe (Egypt). *Microchem. J.* **2005**, *79*, 83–90. [CrossRef]
44. Shillito, L.M.; Almond, M.J.; Wicks, K.; Marshall, L.J.R.; Matthews, W. The Use of FT-IR as a Screening Technique for Organic Residue Analysis of Archaeological Samples. *Spectrochim. Acta A Mol. Biomol. Spectrosc.* **2009**, *72*, 120–125. [CrossRef] [PubMed]
45. Madejová, J. FTIR Techniques in Clay Mineral Studies. *Vib. Spectrosc.* **2003**, *31*, 1–10. [CrossRef]
46. Schwanninger, M.; Rodrigues, J.C.; Pereira, H.; Hinterstoisser, B. Effects of Short-Time Vibratory Ball Milling on the Shape of FT-IR Spectra of Wood and Cellulose. *Vib. Spectrosc.* **2004**, *36*, 23–40. [CrossRef]
47. Fengel, D.; Wegener, G. *Wood: Chemistry, Ultrastructure, Reactions*; Walter de Gruyter: Berlin, Germany, 1983.
48. Poletto, M.; Zattera, A.J.; Santana, R.M.C. Structural Differences between Wood Species: Evidence from Chemical Composition, FTIR Spectroscopy, and Thermogravimetric Analysis. *J. Appl. Polym. Sci.* **2012**, *126*, E337–E344. [CrossRef]
49. Colom, X.; Carrillo, F. Crystallinity Changes in Lyocell and Viscose-Type Fibres by Caustic Treatment. *Eur. Polym. J.* **2002**, *38*, 2225–2230. [CrossRef]
50. Derrick, M.R.; Stulik, D.C.; Landry, J.M. *Infrared Spectroscopy in Conservation Science*; Getty Conservation Institute: Los Angeles, CA, USA, 2000.

51. Faix, O. Classification of Lignins from Different Botanical Origins by FT-IR Spectroscopy. *Holzforschung* **1991**, *45*, 21–27. [CrossRef]
52. Brenneisen, R. Chemistry and Analysis of Phytocannabinoids and Other Cannabis Constituents. In *Marijuana and the Cannabinoids*; Humana Press: Totowa, NJ, USA, 2007.
53. Callaway, J.C. Hempseed as a Nutritional Resource: An Overview. *Euphytica* **2004**, *140*, 65–72. [CrossRef]
54. Gravagna, E. Tracing Provenance of Mesolithic and Neolithic Pottery along the Nile River by Trace Elements and Sr Isotope Analysis. Ph.D. Thesis, University of Padova, Padova, Italy, 2017.
55. Barani, H.; Ghorbani, H.R.; Moradi, F.; Mehrizi, M.M.; Sharifi, M.; Lievens, C. Archaeometric Analysis of Pottery Sherds from Barveh Tepe: Insights into Early Bronze Age Pottery-Making Techniques and Firing Temperatures. *Archaeometry* **2025**, *67*, 328–343. [CrossRef]
56. Ion, R.M.; Pungoi, A.E.; Iancu, L.; Grigorescu, R.M.; Vasilievici, G.; Gheboianu, A.I.; Slamnoiu-Teodorescu, S.; Alexandrescu, E. Compositional and Microstructural Investigations of Prehistoric Ceramics from Southern Romania (Middle Neolithic Pottery). *Appl. Sci.* **2024**, *14*, 5755. [CrossRef]
57. Teodorescu, L.; Amara, A.B.; Cantin, N.; Chapoulie, R.; Ducu, C.; Ciucă, S.; Tulugea, C.; Terteci, C.; Abrudeanu, M. Characterization of Archaeological Artefacts Using Methods Specific to Materials Science: The Case Study of Dacian Ceramics from 2nd c. BC to 1st c. AD. *Materials* **2021**, *14*, 3908. [CrossRef] [PubMed]
58. Drebushchak, V.A.; Mylnikova, L.N.; Molodin, V.I. Thermogravimetric Investigation of Ancient Ceramics. *J. Therm. Anal. Calorim.* **2007**, *90*, 73–79. [CrossRef]
59. Dal Sasso, G.; Maritan, L.; Salvatori, S.; Mazzoli, C.; Artioli, G. Discriminating Pottery Production by Image Analysis: A Case Study of Mesolithic and Neolithic Pottery from Al Khiday (Khartoum, Sudan). *J. Archaeol. Sci.* **2014**, *46*, 125–143. [CrossRef]
60. Tite, M.S. Ceramic Production, Provenance and Use: A Review. *Archaeometry* **2008**, *50*, 216–231. [CrossRef]
61. Tutuk, G.G. Anadolu'da Arkeolojik ve Filolojik Veriler Işığında Tekstil Teknolojisinin Gelişimi. Bachelor's Thesis, Uludağ University, Bursa, Türkiye, 2020.
62. Yılmaz, D. Geç Tunç Çağı'nda Batı Anadolu'da Tekstil Üretimi: Çine-Tepecik Höyüğü Tezgah Ağırlıkları. *TÜBA-AR Türkiye Bilim. Akad. Arkeol. Derg.* **2016**, *19*, 93–111. [CrossRef]
63. Balcik, H.; Karul, N. Kuzeybatı Anadolu'da Tarımın Başlangıcı: Barçın Höyük Bitki Kalıntıları Üzerine Bir Değerlendirme. Master's Thesis, Sosyal Bilimler Enstitüsü, Istanbul, Türkiye, 2018.
64. Eren, E.; Tosyagülü, Ç.H. Anadolu Coğrafyasında Neolitik Dönem Arkeobotanik Buluntuları. *Karadeniz Uluslararası Bilimsel Dergi* **2023**, *58*, 22–40. [CrossRef]
65. Arie, E.; Rosen, B.; Namdar, D. Cannabis and Frankincense at the Judahite Shrine of Arad. *Tel Aviv* **2020**, *47*, 5–28. [CrossRef]

Disclaimer/Publisher's Note: The statements, opinions and data contained in all publications are solely those of the individual author(s) and contributor(s) and not of MDPI and/or the editor(s). MDPI and/or the editor(s) disclaim responsibility for any injury to people or property resulting from any ideas, methods, instructions or products referred to in the content.